

Egyptian Journal of Chemistry

http://ejchem.journals.ekb.eg/



Improving the Consolidating Efficiency of Acrylic Polymers by Incorporating Silica and Calcium Carbonate Nanoparticles: A Case Study on Fired Bricks at the IbnTulun Aqueduct, Egypt Mahmoud Abd El Hafez Adam^{1, 2,}, Mohamed Shaker³, Shaymaa El-Sayed El- Shafey^{4*},



Sherif Omar²

¹College of Archaeology and Cultural Heritage - The Arab Academy for Science, Technology and Maritime Transport, Egypt,

New Vally branch

²Department of Inorganic Conservation, Faculty of Archaeology, Cairo University, P.O. Box 12613, Giza 12221, Egypt

³MSc Researcher, Department of Inorganic Conservation, Faculty of Archaeology, Cairo University

⁴Surface chemistry and Catalysis Laboratory, Physical Chemistry Department, National Research Centre, 33 El – Bohouth,

P.O. Box 12622, Giza, Egypt

Abstract

The fired bricks of archaeological supply facilities—particularly the Ahmed IbnTulun Aqueduct, dating to the Abbasid period (875 AD)—have received limited attention in terms of integrated conservation. This study aims to identify the main deterioration factors affecting these bricks and to assess the effectiveness of selected nanocomposites for their consolidation and protection. A comprehensive methodology was applied, including examination, analysis, and evaluation using USB digital microscopy, polarized light microscopy (PLM), scanning electron microscopy (SEM), X-ray diffraction (XRD), and Xray fluorescence (XRF). Consolidants were prepared using silica (SiO₂) and calcium carbonate (CaCO₃) nanoparticles (mean particle diameter < 30 nm as confirmed by TEM) at 3% and 5% concentrations, dispersed in an acrylic copolymer matrix (Paraloid B72: 70% ethyl methacrylate, 30% methyl acrylate). Treated, untreated, and artificially aged samples were evaluated for physical and mechanical properties, colorimetric changes, and water contact angle. Quantitative results showed that the SiO₂ /Paraloid B72 nanocomposite at 5% concentration increased compressive strength from 88.05 kg/cm² (untreated) to 231.21 kg/cm², and achieved a static water contact angle of 107°, indicating both enhanced mechanical strength and strong water repellenc.Results demonstrated that both SiO2 and CaCO3 nanocomposites significantly enhanced compressive strength, with the SiO₂ /Paraloid B72 nanocomposite at 3% achieving the best overall performance—particularly in improving water repellency while maintaining the original appearance of the friedbricks, and showing excellent material compatibility and durability properties of prepared materials. The CaCO₃ /Paraloid B72 nanocomposite ranked second in performance; however, the 5% formulation caused slight chromatic alteration and less effective water repellency, indicating the need for concentration adjustments to improve its conservation applicability.

Keywords: Fired brick; Acrylic polymers; Silica nanoparticles; Calcium carbonate nanoparticles; consolidation; Ahmed IbnTulun aqueduct

Introduction

The Tulunid period marked a significant era in the history of Egypt. In 882 AD, Ahmed IbnTulun succeeded in securing Egypt's independence from the Abbasid Caliphate after centuries of subordination [1]. He commissioned the construction of an extensive aqueduct system to supply water to his newly established capital, Al-Qata'i, which was built on elevated terrain, whereas the Nile River flowed at a lower level [2]. The intake tower is the most prominent architectural element of the Ahmed IbnTulun Aqueduct and remains the best-preserved part of this archaeological structure to date (Fig. 1). The intake source of the aqueduct originated from a natural spring in the El-Basateen area, located in what is now southern Cairo. A surviving water-wheel tower, which once played a key role in lifting water into the system, still stands in the Beir Om Al-Sultan neighborhood within the same area [3].

The aqueduct of Ahmed IbnTulun, considered the oldest Islamic hydraulic monument in Egypt, still stands largely preserved with its original construction materials—primarily fired bricks—dating back to the 9th century. This historical structure was originally supplied by two large water wheels that lifted water from a square well to the top of the intake tower, channeling it northeastward to key locations in the Tulunid capital, Al-Qata'i. However, the aqueduct currently suffers from multiple forms of damage and deterioration, including prolonged neglect and urban encroachment, which have led to the removal of some original components. The remaining sections exhibit significant material degradation, such as cracking and erosion of the fired bricks, as well as deterioration of the bonding mortar due to exposure to various weathering agents. Notably, the southern sector of the aqueduct originally extended approximately 870 meters, but only about 540 meters remain today due to extensive destruction[4, 5].

*Corresponding author e-mail: s_shafey@yahoo.com; Mahmoud Adam

Received Date: 23 June 2025, Revised Date: 19 July 2025, Accepted Date: 26 August 2025

DOI: 10.21608/EJCHEM.2025.396868.11947

©2026 National Information and Documentation Center (NIDOC)

466 M. Adam et.al.



Fig. 1.The four façades of the intake tower of the Ahmed IbnTulun Aqueduct: (A) Eastern (main) façade; (B) Western façade; (C) Northern façade; (D) Southern façade. (Photographs taken by the authors).

The aqueduct of Ahmed IbnTulun, considered the oldest Islamic hydraulic monument in Egypt, still stands largely preserved with its original construction materials—primarily fired bricks—dating back to the 9th century. This historical structure was originally supplied by two large water wheels that lifted water from a square well to the top of the intake tower, channeling it northeastward to key locations in the Tulunid capital, Al-Qata'i. However, the aqueduct currently suffers from multiple forms of damage and deterioration, including prolonged neglect and urban encroachment, which have led to the removal of some original components. The remaining sections exhibit significant material degradation, such as cracking and erosion of the fired bricks, as well as deterioration of the bonding mortar due to exposure to various weathering agents. Notably, the southern sector of the aqueduct originally extended approximately 870 meters, but only about 540 meters remain today due to extensive destruction[4, 5].

The deterioration of ancient fired brick masonry is driven by a range of environmental and material factors. One of the principal issues is brick weathering, which can result in surface disintegration and the formation of powdery residues. This process is often exacerbated by elevated moisture levels, leading to salt efflorescence that further compromises the structural integrity of the bricks. Additionally, the binding mortar commonly deteriorates, losing cohesion and contributing to the overall weakening of the masonry system. The combined impact of these factors represents a major threat to the preservation of historic brick structures [6]. In the case of the aqueduct, neglect and encroachment over recent years have been accompanied by demolition and structural damage. Field observations revealed that the exposed surfaces of the bricks had disintegrated into powder, with visible salt crystallization caused by high humidity levels, and significant deterioration of the bonding mortar (Fig. 2).

cultural identity and reflect the architectural and technological achievements of ancient civilizations. Accordingly, the integration and adaptation of modern technologies and materials are essential in the conservation process. In recent years, nanotechnology has significantly enhanced the performance of various materials used in the consolidation and preservation of both fired bricks and mortars.

Moreover, several previous studies have explored different concentrations of CaCO₃ nanoparticles and other types of nanoparticles—typically ranging from 1% to 10%—incorporated into polymeric materials[7]. In the present study, silica and calcium carbonate nanoparticles were used at varying concentrations within an acrylic copolymer matrix to consolidate archaeological fired bricks. The selection of treatment materials was guided by prior research that investigated diverse strategies for the incorporation and dispersion of nanoparticles in polymer systems [8]. These studies generally concluded that the optimal nanoparticle concentration falls between 3% and 7% of the polymer content [9, 10]. Accordingly, the objective of the current experimental work was to evaluate the most effective nanocomposite formulation for the consolidation and protection of archaeological fired brick samples.

This study focuses on the Ahmed IbnTulun Aqueduct and its current condition as an endangered archaeological site. It includes an experimental investigation of the fired bricks used in its construction, aiming to identify their physicochemical and mechanical properties, as well as the nature and causes of their deterioration. Based on these findings, the study assesses the present state of conservation and evaluates appropriate restoration materials and intervention strategies. Special emphasis is placed on nanotechnology-based methods, as the research examines the effectiveness of selected nanocomposites in consolidating the fired bricks and enhancing their durability to support the sustainable preservation of the monument[7, 11]. Therefore, the main objectives of this study are: (1) to diagnose the deterioration mechanisms affecting the fired bricks, and (2) to evaluate the performance of SiO₂ and CaCO₃ -based nanocomposites at different concentrations in terms of mechanical enhancement, water repellency, and material compatibility.

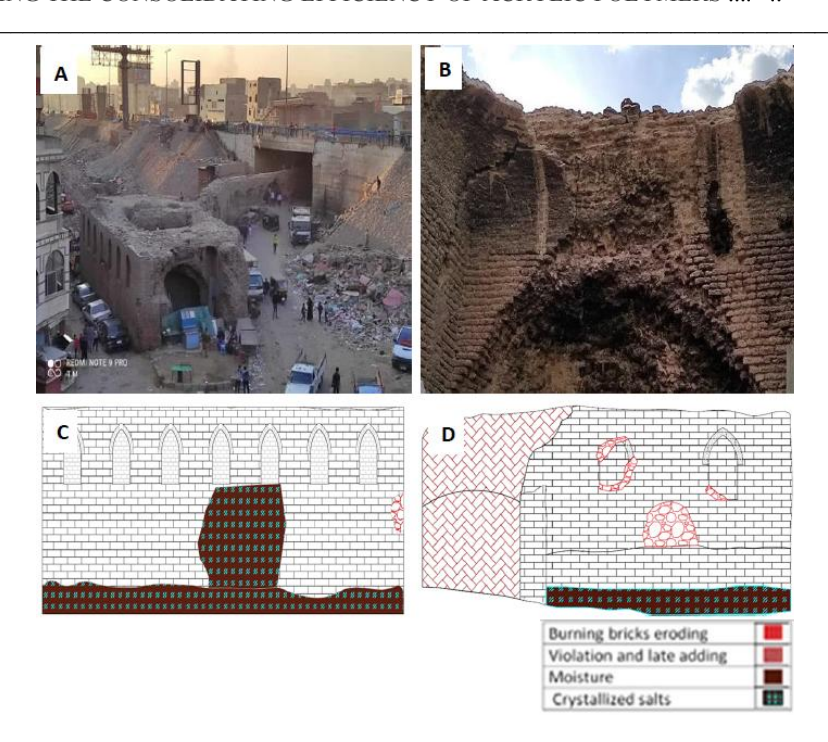


Fig. 2. Current Condition and Deterioration Features of the Ahmed IbnTulun Aqueduct: (A) General view of the site and the surrounding urban and residential environment of the intake tower, showing overall degradation and human encroachment on the archaeological context; (B) Eastern (main) façade of the intake tower, exhibiting severe deterioration, disintegration of fired bricks, multiple cracks, and partial collapse; (C) AutoCAD drawing illustrating selected deterioration patterns on the southern façade of the intake tower; (D) Engineering drawing highlighting deterioration on the western façade, including material degradation, wall saturation due to moisture, and signs of human interference through the addition of modern structures. (Photographs and drawings by the authors)

2. Materials and Methods

2.1. Materials

2.1.1. Archaeological samples

The studied aqueduct of Ahmed IbnTulun was primarily constructed using fired bricks. Due to prolonged exposure to various physical, chemical, and mechanical factors, several brick components became detached and disintegrated. For the purposes of this study, a set of detached brick samples was carefully collected from different areas of the intake structure, ensuring that no damage or loss was inflicted upon the archaeological value of the site. The samples were taken from the eastern façade (main entrance), as well as the northern, southern, and western façades. Each sample was labeled and coded for clear identification throughout the study[12].

2.1.2. Experimental Fired Brick Samples

The experimental fired brick samples, collected from fallen components of the archaeological site, were cut into $3 \times 3 \times 3$ cm cubes, thoroughly cleaned, and oven-dried at 105 °C for 24 hours. Subsequently, the samples were left to air-dry at room temperature for an additional 21 days [13].

2.1.3. Treatment and Protection Products

The acrylic copolymer Paraloid B72 is one of the most widely used polymers in the conservation of building materials. It consists of ethyl methacrylate (70%) and methyl acrylate (30%). This copolymer has been employed for decades in the reinforcement and consolidation of historic construction materials. In the present study, Paraloid B72 was dissolved in acetone at a concentration of 3% [14, 15].

Nanosilica powder (SiO_2) was incorporated into Paraloid B72 at concentrations of 3% and 5% (w/v), and similarly, nano-calcium carbonate powder ($CaCO_3$) was added at the same concentrations [16, 17]. The nanocomposites were prepared by directly mixing the polymer solution with the nanoparticles. The preparation method involved dispersing silica and calcium carbonate nanoparticles in an aqueous suspension of 3% (w/v) acrylic copolymer. The mixtures were maintained at 75 °C under continuous mechanical stirring. Subsequently, the compositions were further homogenized using mechanical blending followed by sonication for 2 hours. The final nanocomposites were applied to the brick samples by brushing under ambient temperature and pressure. The consolidation process was repeated three times, with one-hour intervals between applications. All nanomaterials and nanocomposite preparations were carried out at the Polymer Laboratory, National Research Centre, Dokki, Egypt [18, 19]. Table 1 presents the concentrations of nanocomposites used in the consolidation of the archaeological fired brick samples.

468 M. Adam et.al.

It is important to note that the properties of the four nanocomposites were evaluated to assess their compatibility with fired brick substrates and to ensure that they would not adversely affect the physical characteristics of the treated samples. Following the application of the consolidants, the specimens were left to dry under ambient conditions for one month to allow complete curing [20, 21].

Table 1. Concentrations of nanocomposites used in consolidation of the archeological fired brick samples

| Treatment materials | Concentration (%) | Nano solid content (g) | Polymer solid content (g) | Resultingnanocomposi te |
|------------------------------------|-------------------|------------------------|---------------------------|---|
| Paraloid B72 | 3 | _ | 7.59 | _ |
| SiO ₂ nanoparticles | 3 | 0.22 | 7.59 | SiO ₂ / B72 Nanocomposite (3%) |
| SiO ₂ nanoparticles | 5 | 0.37 | 7.59 | SiO ₂ / B72 Nanocomposite (5%) |
| CaCO ₃ nanoparticles | 3 | 0.22 | 7.59 | CaCO ₃ / B72 Nanocomposite (3%) |
| CaCO ₃ nanoparticles | 5 | 0.37 | 7.59 | CaCO ₃ / B72 Nanocomposite (5%) |

2.1.4. Artificial Aging

This test is typically conducted to evaluate the durability of treated samples by subjecting them to accelerated stress conditions, simulating potential future exposure to environmental factors such as climate fluctuations and harsh atmospheric influences. Temperature and moisture variations are considered among the most critical agents of deterioration in archaeological building materials. Therefore, the treated samples were subjected to ten consecutive aging cycles, each consisting of 18 hours of immersion in distilled water followed by 6 hours of drying at 105 °C. After completing the cycles, the samples were left at room conditions before subsequent measurements were carried out [13, 22].

2.2. Methods

2.2.1. Examination and Analysis Techniques

2.2.1.1. USB Digital Microscopy

The collected samples were initially examined using a USB digital microscope (Win7/Vista/XP, $40 \times -500 \times$ magnification) to document and characterize their surface features. The device is equipped with a dynamic image sensor (2×2 CMOS) and eight bright white LED lights, enabling the capture of high-resolution images directly onto a computer screen.

2.2.1.2. Polarized Light Microscopy (PLM)

The samples were examined using a polarized light microscope (Nikon Optiphot X23) under 10^{\times} and 20^{\times} magnifications in plane-polarized light mode [23].

2.2.1.3. Scanning Electron Microscopy (SEM)

A field emission scanning electron microscope (FE-SEM), model TESCAN VEGA3, with a resolution of $0.6\,\mathrm{nm}$ at $15\,\mathrm{kV}$ and $1.0\,\mathrm{nm}$ at $1\,\mathrm{kV}$, was used to examine the morphology of the experimental fired brick samples before and after treatment.

2.2.1.4. Transmitted Electron Microscopy (TEM)

 SiO_2 and $CaCO_3$ nanoparticles were characterized using a transmission electron microscope (TEM), model Tecnai G20 SuperTwin, equipped with a double-tilt holder. The instrument operated at an accelerating voltage of 200 kV, using a lanthanum hexaboride (LaB₆) electron source. Imaging was conducted in both bright-field mode and selected area electron diffraction (SAED) to analyze the morphology and crystallinity of the nanoparticles.

2.2.1.5. X ray Diffraction Analysis (XRD)

Standard fired brick samples were analyzed using X-ray diffraction (XRD) to identify their mineralogical composition. The analysis was performed using a Philips PW 3071 diffractometer with $CuK\alpha$ radiation at 40 kV and 30 mA.

2.2.1.6. X ray Fluorescence Analysis (XRF)

X-ray fluorescence (XRF) analysis is a fundamental technique for determining the elemental composition of archaeological fired brick samples. The analysis was carried out at the laboratories of the Egyptian Mineral Resources Authority using a PANalyticalAxios spectrometer (model 2005).

2.2.2. Physical and Mechanical Properties

The water absorption test was conducted as a key indicator of thefriedbricks' resistance to freeze—thaw cycles, providing essential information on their durability. Initially, the samples were cleaned of impurities, dried, and their dry weights were recorded. Subsequently, the samples were immersed in water for 48 hours, after which their saturated weights were measured. In addition, the bulk density and porosity of untreated, treated, and artificially aged samples were calculated in accordance with UNI 10859:2000 [24, 25].

The compressive strength test was performed on fired brick samples before and after treatment to evaluate their mechanical performance. The test was conducted using an Amsler compression testing machine, with the load applied perpendicular to the bedding plane, in accordance with ASTM C170. The average compressive strength values were recorded for the untreated, treated, and artificially aged samples [26]

2.2.3. Colorimetric Measurements

Color changes in the fired brick specimens were measured using a CM-2600d Konica Minolta spectrophotometer (New York, USA) to assess chromatic variations before and after treatment, as well as following artificial thermal aging. Chromatic values were recorded in the CIE Lab* color space, where L* represents lightness (ranging from black to white), a* corresponds to the red–green axis (+a* indicating red, -a* green), and b* corresponds to the yellow–blue axis (+b* indicating yellow, -b* blue) [27]

2.2.4. Static Water Contact Angle Measurements

The static water contact angle of the fired brick samples was measured before and after treatment to assess their hydrophobicity and surface stability. The test was carried out using a custom-designed apparatus developed in accordance with UNI EN 15802:2010. Contact angle measurements were captured using a high-resolution Canon camera fitted with an 18–55 mm lens [28].

3. Results and Discussion

3.1. Characterization of Fired Bricks by USB Digital Microscopy

USB digital microscopy revealed quartz grains of varying sizes embedded within the fired brick matrix. Iron oxide particles were also observed, appearing as reddish inclusions dispersed throughout the samples (Fig. 3A, B). Additionally, numerous pores of different sizes were detected, most likely resulting from salt weathering processes that contributed to microstructural degradation (Fig. 3C, D).

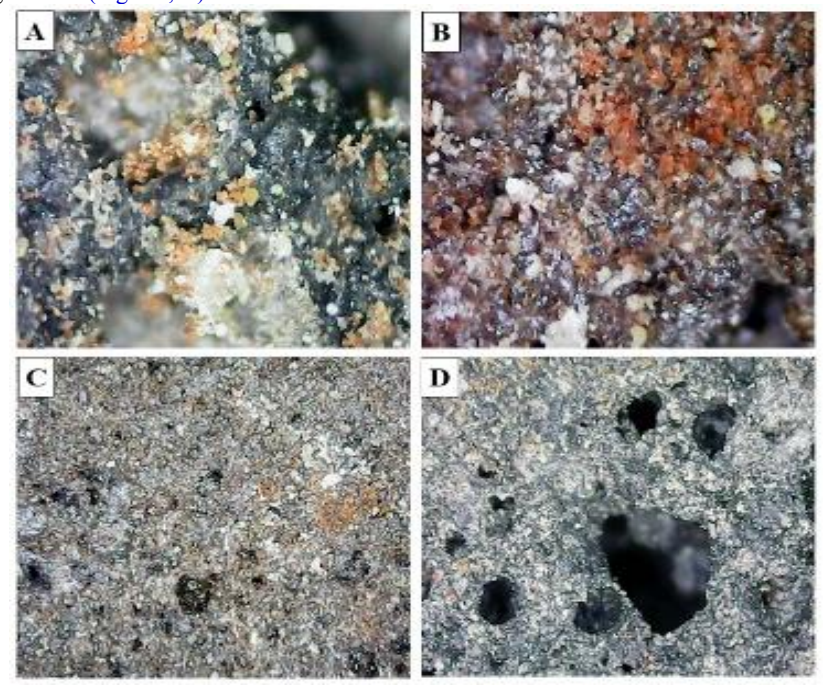


Fig. 3. USB microscopy results: (A) Quartz grains with varying sizes $(500\times)$; (B) Iron oxide inclusions observed in the analyzed samples $(300\times)$; (C, D) Pores of different sizes identified in the samples $(300\times)$ and $400\times$, respectively).

3.2. Diagnosis by Polarized Light Microscopy (PLM)

The fired brick samples were examined and characterized using polarized light microscopy (PLM), as illustrated in Fig. 4. The analysis revealed that the archaeological brick matrix is primarily composed of quartz and feldspar grains—mainly anorthite and labradorite—alongside minor amounts of clay minerals. These components are embedded in a matrix rich in iron oxides, with occasional traces of carbonates. Quartz occurs as very fine, sand- to silt-sized grains, ranging from subrounded to angular in shape, often associated with clay minerals and iron oxide accumulations.

Feldspar minerals appear as fine-grained, subhedral crystals distributed throughout various regions of the sample, while mafic minerals are present as fine, prismatic crystals. The clay minerals exhibit clear deformation, likely due to thermal alteration during the firing process. Some areas of the samples are visibly stained by iron oxides. Additionally, the fired bricks display high porosity, characterized by abundant irregular pores and cavities, which are attributed to weathering processes occurring over time at the archaeological site.

Fig. 4. PLM photomicrographs of the studied fired brick samples: (A, B) The mineral composition of the bricks and phase transformations resulting from the firing process are clearly visible. Thin sections also reveal voids and pores associated with weathering processes that affected the bricks at the archaeological site (25×, cross-polarized light).

3.3. Scanning Electron Microscopy (SEM)

Scanning electron microscopy (SEM) of the untreated archaeological samples revealed significant deterioration, the absence of binding materials, mineral alteration, and the presence of microcracks. Extended exposure to acidic saline weathering and deep pits of varying sizes physical damage (Fig. 5A). The B72/nanosilicananocompositepenetrated effectively into the brick's porous structure. It formed a continuous film and improved surface cohesion, as confirmed by SEM analysis.

(Fig. 5B). This nanocomposite also exhibited minimal degradation following artificial aging processes involving heat and humidity (Fig. 5C).

Similarly, SEM observations indicated that the Paraloid B72/nanosilica 5% nanocomposite also achieved deep and homogeneous penetration into internal cracks and voids, with the consolidant appearing evenly distributed across the microstructure (Fig. 5D). The nanocomposite maintained its structural coherence and uniformity after artificial aging, reinforcing its efficiency and durability (Fig. 5E).

On the other hand, the Paraloid B72/nanocalcite 3% nanocomposite successfully formed a homogeneous polymeric coating over the mineral grains, with branched nanostructures indicating complete encapsulation. However, some fine cracks and fissures were still observed (Fig. 5F). The nanocomposite retained its stability and cohesion after artificial aging (Fig. 5G). Furthermore, SEM analysis of the Paraloid B72/nanocalcite 5% nanocomposite revealed a homogeneous distribution across mineral grains and within internal cracks and pores. It also appeared in the form of nanostructured protrusions, while preserving some fine open pores, indicating that the treatment did not result in complete pore blockage (Fig. 5H). This nanocomposite also demonstrated a high degree of stability following artificial aging (Fig. 51)

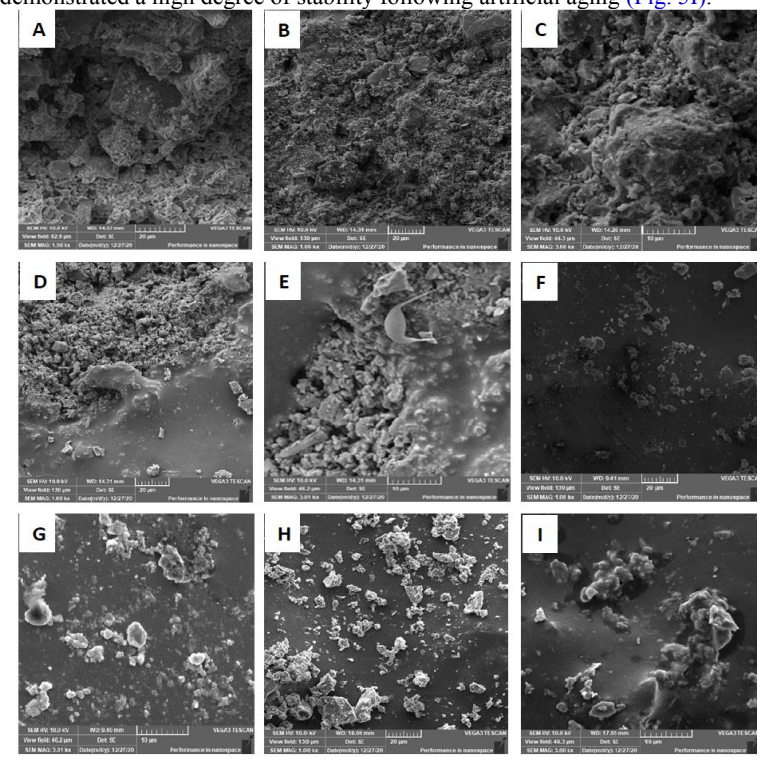


Fig. 5. SEM photomicrographs of the studied archaeological fired brick samples: (A) Untreated sample; (B) Sample treated with Paraloid B72/nanosilica 3% nanocomposite; (C) Same as (B) after artificial aging; (D) Sample treated with Paraloid B72/nanosilica 5%; (E) Same as (D) after artificial aging; (F) Sample treated with Paraloid B72/nanocalcite 3%; (G) Same as (F) after artificial aging; (H) Sample treated with Paraloid B72/nanocalcite 5%; (I) Same as (H) after artificial aging.

3.4. Transmitted Electron Microscopy (TEM)

Transmission electron microscopy (TEM) was used to characterize the particle size of silica and calcium carbonate (calcite) nanoparticles prior to their incorporation into the Paraloid B72 polymer matrix. TEM images revealed that the mean particle diameter was less than 30 nm (Fig. 6A–D).

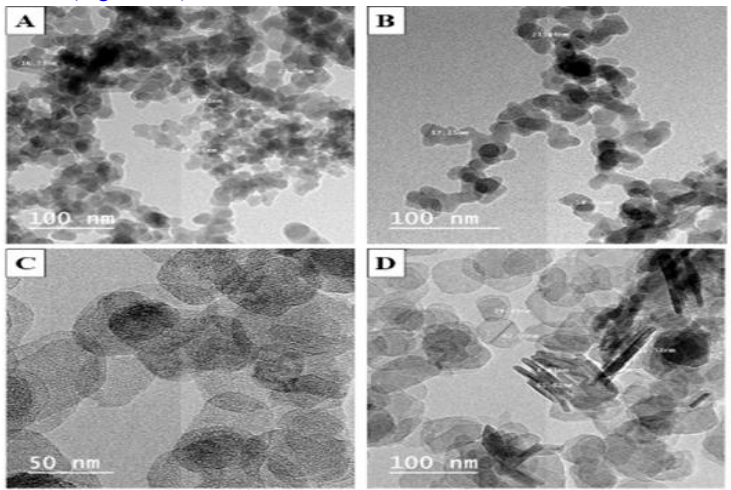


Fig. 6. TEM micrographs of the investigated nanoparticles: (A, B) silica nanoparticles; (C, D) calcium carbonate (calcite) nanoparticles.

3.5. X ray Diffraction Analysis (XRD)

Two samples of archaeological fired brick, collected from the lower portions of the eastern (main) and western façades of the intake tower, were analyzed using X-ray diffraction (XRD). The XRD results for the sample from the eastern façade revealed the presence of quartz (SiO₂) at approximately 50%, anorthite (CaAl₂ Si₂ O₈) at around 40%, and iron oxides—mainly hematite (Fe₂ O₃)—at 15%, along with minor traces of halite (NaCl) as a salt contaminant (Fig. 7A). In contrast, the sample from the western façade exhibited albite (NaAlSi₃ O₈) as the dominant phase (50%), followed by quartz (SiO₂) at 40%, and a minor amount of actinolite (Ca₂ (Mg,Fe)₅ Si₈ O_{2 2} (OH)₂) (Fig. 7B).

The XRD data indicate that the fired bricks contain a high proportion of sand-based material, consistent with the dominance of quartz. Additionally, the presence of halite crystals suggests prolonged exposure to groundwater infiltration, leading to salt crystallization within the brick matrix—a key factor in the deterioration of historic masonry structures over time [²⁹].

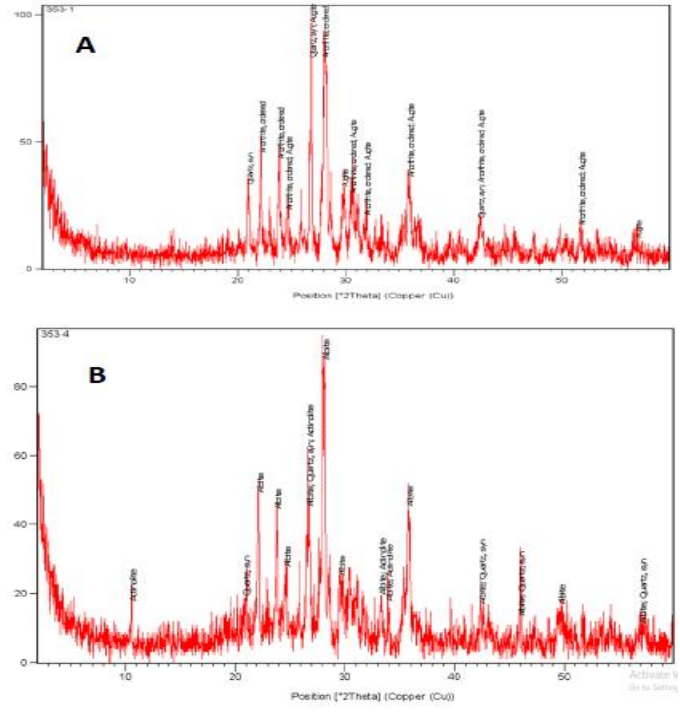


Fig. 7. XRD patterns of archaeological fired brick samples: (A) Sample from the eastern façade of the intake tower, showing dominant peaks of quartz (SiO₂), anorthite (CaAl₂ Si₂ O₈), and iron oxides (Fe₂ O₃), along with minor traces of halite (NaCl); (B) Sample from the western façade, characterized by the presence of albite (NaAlSi₃ O₈), quartz (SiO₂), and a minor amount of actinolite (Ca₂ (Mg,Fe)₅ Si₈ O_{2 2} (OH)₂).

3.6. X ray Fluorescence Analysis (XRF)

472

Table 2 presents the results of X-ray fluorescence analysis (XRF) of the two samples of archaeological fired brick (referred to in the X-ray diffraction analysis). As presented in Table 2, both brick samples show high SiO_2 content (over 51%), followed by significant levels of Al_2 O_3 , Fe_2 O_3 , and CaO. Notable differences include higher Na_2 O and Cl in Sample A, and higher CaO and Fe_2 O_3 in Sample B. The XRF analysis of the two fired brick samples supports the mineralogical findings identified by XRD. Sample A (from the eastern façade) shows a higher content of SiO_2 (52.91%) and Na_2 O (1.72%), which is consistent with the dominance of quartz (SiO_2) and traces of halite (NaCl) detected via XRD. The relatively elevated levels of Al_2 O_3 (13.25%) and CaO (6.79%) reflect the presence of anorthite ($CaAl_2$ Si_2 O_8), a common feldspathic phase formed during the firing of clay-rich materials.

Sample B (from the western façade) is characterized by a slightly lower SiO_2 content (51.31%) but shows a notably higher CaO concentration (9.25%) and lower Na_2 O (0.78%), which aligns with the XRD identification of albite (NaAlSi₃ O₈) and reduced halite content. The higher Fe_2 O₃ content (14.45%) in this sample may contribute to its reddish coloration and suggests greater incorporation of iron oxides during brick formation.

Both samples show similar contents of TiO_2 , MgO, and K_2 O, indicating they originate from the same clay source. In contrast, Sample A contains a significantly higher Cl level (2.12%), along with differences in SO_3 content. This suggests contamination by salts, most likely due to groundwater exposure. These findings support the conclusion that salt crystallization was a major contributor to physical deterioration observed in the SEM and macroscopic examinations

| Table 2. XRF elemental comp | position of fired brick samp | oles: Sample A (eastern f | facade) and Sample B | (western facade). |
|------------------------------------|------------------------------|---------------------------|----------------------|-------------------|
|------------------------------------|------------------------------|---------------------------|----------------------|-------------------|

| Oxide composition (wt%) | Sample (A) | Sample (B) | | |
|--------------------------------|------------|------------|--|--|
| SiO ₂ | 52.91 | 51.31 | | |
| TiO ₂ | 2.54 | 2.53 | | |
| Al_2O_3 | 13.25 | 12.68 | | |
| Fe ₂ O ₃ | 13.79 | 14.45 | | |
| MnO | 0.21 | 0.24 | | |
| MgO | 2.49 | 2.51 | | |
| CaO | 6.79 | 9.25 | | |
| Na ₂ O | 1.72 | 0.78 | | |
| K ₂ O | 1.69 | 1.57 | | |
| P ₂ O ₅ | 0.36 | 0.32 | | |
| Cl | 2.12 | 1.17 | | |
| SO ₃ | 0.01 | 0.14 | | |

3.7. Physical and Mechanical Properties

The results presented in the Table 3 clearly demonstrate the impact of nanocomposite treatments on the physical properties of the archaeological fired brick samples. Compared to the untreated reference, all treated samples exhibited increased density and reduced porosity and water absorption, indicating an overall improvement in consolidation effectiveness. Among the tested nanocomposites, SiO₂ /polymer at 3% concentration showed the most balanced performance, achieving a significant reduction in porosity (15.11%) and water absorption (8.90%), while maintaining a moderate density (1.43 g/cm³). This suggests efficient penetration and compatibility with the internal microstructure of the friedbricks. In contrast, the 5% SiO₂ nanocomposite yielded the highest density (1.59 g/cm³), but with higher porosity and water absorption values compared to the 3% formulation, possibly due to surface film formation or reduced penetration at higher nanoparticle loading.

The $CaCO_3$ /polymer nanocomposites exhibited less pronounced improvement. While the 3% formulation showed comparable porosity to the untreated sample (22.30%), its absorption remained relatively high (14.30%), suggesting limited pore filling or weaker bonding capacity. The 5% $CaCO_3$ composite performed slightly better, but still less effectively than the silica-based systems.

After artificial aging, all treated samples showed acceptable stability, with moderate increases in porosity and water absorption. These changes likely result from both environmental degradation and inherent material properties, such as the original firing conditions and clay composition. The $3\% \, \mathrm{SiO_2}$ /polymer nanocomposite maintained the best hydrophobicity, with post-aging water absorption as low as 10.80%, indicating excellent long-term durability and moisture resistance.

| Table 3. Average values of physical | properties for untreated, treated | l, and artificially aged fired brick samples. |
|-------------------------------------|-----------------------------------|---|
| | | t' |

| Nanocomposite | | After treatn | ient | After artificial aging | | | |
|--|-------------------------------|--------------|----------------------------|--------------------------------|--------------|----------------------------|--|
| | Density gm/cm ³ | Porosity (%) | Water absorption (%) | Density gm/c m ³ | Porosity (%) | Water absorption (%) | |
| Untreated sample (Standard) | 1.19 | 22.50 | 18.13 | - | 2 | - | |
| SiO ₂ /polymer Nanocomposites (3% concentration) | 1.43 | 15.11 | 8.90 | 1.37 | 14.62 | 10.80 | |
| SiO ₂ /polymer Nanocomposites (5% concentration) | 1.59 | 21.89 | 11.23 | 1.50 | 20.91 | 13.80 | |
| CaCO ₃ /polymer Nanocomposites (3% concentration) | 1.35 | 22.30 | 14.30 | 1.27 | 22.23 | 15.37 | |
| CaCO ₃ /polymer Nanocomposites (5% concentration) | 1.32 | 21.86 | 14.10 | 1.29 | 19.23 | 15.14 | |

The compressive strength results presented in the Table 4 clearly highlight the enhancement achieved through nanocomposite treatment. Compared to the untreated sample ($88.05 \, \text{kg/cm}^2$), all treated samples exhibited improved strength, with the SiO_2 /polymer nanocomposite at 5% concentration showing the most significant increase ($231.21 \, \text{kg/cm}^2$). Even after artificial aging, this sample maintained the highest mechanical performance ($219.40 \, \text{kg/cm}^2$), indicating strong consolidation and long-term stability. The $3\% \, \text{SiO}_2$ /polymer treatment also improved strength moderately ($117.12 \, \text{kg/cm}^2$), aligning with its previously noted physical performance—balanced porosity reduction and good hydrophobicity.

In contrast, the CaCO₃ /polymer nanocomposites showed limited mechanical enhancement, particularly at 3% concentration (70.88 kg/cm²), which remained below the untreated sample. The 5% CaCO₃ composite performed better (89.06 kg/cm²), but still with marginal improvement.

These findings are consistent with the physical property results, where SiO_2 -based nanocomposites demonstrated better densification, lower porosity, and improved water resistance—factors directly contributing to mechanical integrity. The ability of the SiO_2 5% nanocomposite to maintain strength post-aging confirms its superior durability and effectiveness in preserving the structural integrity of archaeological fired bricks.

Table 4. Average compressive strength values of untreated, treated, and artificially aged fired brick samples.

| Nanocomposite | Compressive strength Kg/Cm ² | | | | | |
|---|---|--------------------|------------------------|--|--|--|
| | Untreated sample | After treatment | After artificial aging | | | |
| Untreated sample (Standard) | 88.05 | - | - | | | |
| SiO ₂ /polymer Nanocomposites (3% concentration) | | 117.12 | 104.70 | | | |
| SiO ₂ /polymer Nanocomposites (5% concentration) | | 231.21 | 219.40 | | | |
| CaCO ₃ /polymer Nanocomposites (3% concentration) | | 70.88 | 69.29 | | | |
| CaCO ₃ /polymer Nanocomposites (5% concentration) | | 89.06 | 84.79 | | | |

3.8. Colorimetric Measurements

Colorimetric measurements were performed using an OptiMatch 3100 spectrophotometer to evaluate chromatic variations in the treated and artificially aged brick samples relative to the untreated reference. The total color difference (ΔE) was calculated according to the CIE Lab* color space using the equation [30]:

 $\Delta E = \sqrt{(\Delta L^2 + \Delta a^2 + \Delta b^{*2})}$

According to the Italian guidelines for the restoration of archaeological materials, a ΔE value below 5 is generally considered acceptable, indicating that no significant visual alteration has occurred.

The results confirmed that all SiO_2 /polymer nanocomposite treatments—both at 3% and 5% concentrations—produced ΔE values below the threshold, even after artificial aging (ranging from 2.77 to 4.01), suggesting excellent visual compatibility and chromatic stability. In contrast, the $CaCO_3$ /polymer treatment at 3% exceeded the acceptable limit ($\Delta E = 5.21$), and further increased after aging ($\Delta E = 6.42$), indicating noticeable color change. The 5% $CaCO_3$ formulation remained within the acceptable range before and after aging (3.81 and 4.05, respectively), though with values close to the threshold (Table 5).

These results reinforce the suitability of SiO₂ -based nanocomposites in preserving the original visual appearance of archaeological fired bricks, while highlighting the limitations of lower-concentration CaCO₃ formulations in terms of chromatic alteration.

Table 5. Total color difference (ΔE) values of treated and artificially aged fired brick samples.

| Nanocomposite | Δ (Treated samples) | | | Δ (Artificial aged samples) | | | | |
|--|---------------------|------|------|-----------------------------|------|------|------|------|
| | ΔL* | Δa* | Δb* | Δ E* | ΔL* | Δa* | Δ b* | Δ E* |
| SiO ₂ /polymer Nanocomposites (3% concentration) | 2.61 | 7.41 | 1.64 | 2.77 | 2.90 | 6.41 | 0.93 | 3.06 |
| SiO ₂ /polymer Nanocomposites (5% concentration) | 2.83 | 9.22 | 1.34 | 3.27 | 2.91 | 3.10 | 5.71 | 4.01 |
| CaCO ₃ /polymer Nanocomposites (3% concentration) | 4.29 | 1.70 | 2.08 | 5.21 | 2.91 | 2.21 | 2.30 | 6.42 |
| CaCO ₃ /polymer Nanocomposites (5% concentration) | 3.94 | 5.11 | 7.88 | 3.81 | 4.30 | 7.86 | 1.05 | 4.05 |

3.9. Static Water Contact Angle Measurements

The static water contact angle test was performed to evaluate the surface hydrophobicity of fired brick samples treated with three selected nanocomposites. The nanocalcite/polymer nanocomposite at 3% concentration was excluded from this test due to its unacceptable chromatic alteration, which disqualifies it for conservation purposes.

The contact angle (θ) reflects the wetting behavior of the treated surface. A value below 90° indicates low hydrophobicity and high wettability, allowing water to spread across the surface. In contrast, angles exceeding 90° signify enhanced hydrophobicity, where water tends to bead on the surface, forming a protective barrier [31, 32]

After treatment, the ${\rm SiO_2}$ /polymer nanocomposites at 3% and 5% concentrations recorded contact angles of 102° and 107° , respectively, indicating strong water repellency. The ${\rm CaCO_3}$ /polymer nanocomposite at 5% concentration showed a slightly lower angle of 99°, which is still within the hydrophobic range.

Following artificial aging, a slight decrease in contact angle was observed for all samples. The SiO_2 /polymer 3% sample maintained high hydrophobicity (99°), while the 5% SiO_2 formulation dropped to 87°, falling below the hydrophobic threshold. The $CaCO_3$ /polymer 5% sample exhibited a minor reduction to 93°, indicating moderate but stable water-repellent behavior (Table 6).

These results highlight the superior long-term performance of the SiO_2 /polymer nanocomposite at 3%, which preserved its hydrophobic properties even after accelerated aging conditions.

Table 6. Static water contact angle values of treated and artificially aged fired brick samples.

| Nanocomposite | Static water c | ontact angle (θ) | Contact angle images | | |
|--|--------------------|------------------------|---|--|--|
| | After treatment | After artificial aging | Contact angle images after artificial aging | | |
| SiO ₂ /polymer Nanocomposites (3% concentration) | 102° | 99° | 65.62° ASSEC | | |
| SiO ₂ /polymer Nanocomposites (5% concentration) | 107° | 87° | | | |
| CaCO ₃ /polymer Nanocomposites (5% concentration) | 99º | 93° | 97.89* | | |

4. Conclusion

This study evaluated the use of SiO₂ and CaCO₃ -based nanocomposites with concentrations of 3% and 5% in consolidating the deteriorated fired bricks of the Ahmed IbnTulun Aqueduct. Both materials enhanced the mechanical and hydrophobic properties of the bricks; however, the 3% SiO₂ /Paraloid B72 nanocomposite demonstrated superior performance. It achieved higher compressive strength, excellent water repellency (contact angle: 102°), and minimal color change—indicating strong compatibility with historical materials. In contrast, the 5% CaCO₃ formulation showed reduced efficiency and caused slight chromatic alteration. These findings support the use of low-concentration silica nanocomposites as an effective conservation approach for endangered archaeological brick work. Further research could explore optimizing nanoparticle types and concentrations to tailor treatments for different conservation needs.

5. Conflicts of interest

The authors confirm that no competing interests are associated with this research.

6. Acknowledgment

The authors would like to extend their sincere gratitude to the Arab Academy for Science, Technology and Maritime Transport, the Department of Inorganic Conservation, Faculty of Archaeology, Cairo University, and the Surface Chemistry and Catalysis Laboratory at the National Research Centre for their valuable support, technical collaboration, and continued encouragement

7. References

- [1] Shafei, F. Arab Architecture in Islamic Egypt, Rulers Period, The Egyptian Book Authority: Cairo, 1994; p 512.
- [2] Maher, S. The Mosques of Egypt and Their Righteous Guardians of Peace, Part 1; 1971; p 141.
- [3] Fahimy, A. R. *Cairo and Its History, Arts, and Archaeology*, rev. Hassan Al-Basha; Al Ahram Foundation: Cairo, 1970; p 20.
- [4] Nawar, S. The Water Facilities in Egypt from the Islamic Conquest Until the End of the Mamluk Era, Dar Al-Wafa: Cairo, 1994.
- [5] Shawkat, Y. Destruction Alert: IbnTulun Aqueduct in Basateen. Cairo Observer, 2024. Retrieved from https://cairobserver.com/post/16766637427/destruction-alert-ibn-tulun-aqueduct-in-basateen
- [6] Ashurst, J.; Dimes, F. G. Conservation of Building and Decorative Stone, Butterworth-Heinemann: London, 1990.
- [7] Tang, X.; Yu, F.; Guo, W.; Wang, T.; Zhang, Q.; Zhang, X.; Pei, M. A Facile Procedure to Fabricate Nano Calcium Carbonate Polymer-Based Superhydrophobic Surfaces. *New J. Chem.* 2014, *38*, 2245–2249
- [8] Mansour, S. Comparative Study to Evaluate Efficiency of Conventional Composites and Nanocomposites in Cleaning and Self-Protection for Some Archaeological Stone Surfaces, Applied on Selected Objects, M.Sc. Thesis, Department of Conservation, Faculty of Archaeology, Cairo University: Giza, Egypt, 2014.
- [9] Hong, R. A.; Chen, Q. *Dispersion of Inorganic Nanoparticles in Polymer Matrices: Challenges and Solutions*, Res. Gate, 2015. Retrieved from https://www.researchgate.net/publication/278394214-Advances in Polymer Science
- [10] Buasri, A.; Chaiyut, N.; BorvorAchetarnwat, K.; Chantanachai, N.; Thorglor, K. Thermal and Mechanical Properties of Modified CaCO₃ /PP Nanocomposites. *Int. J. Chem. Mol. Nucl. Metall. Eng.* 2012, 6, 1–4.
- [11] Tang, X.; Yu, F.; Guo, W.; Wang, T.; Zhang, Q.; Zhang, X.; Pei, M. A Facile Procedure to Fabricate Nano Calcium Carbonate Polymer-Based Superhydrophobic Surfaces. *New J. Chem.* 2014, *38*, 2245–2249.
- [12] Dimitrijevic, M.; Karabasil, N.; Boskovic, M.; Teodorovic, V.; Vasilev, D.; Djordjevic, V.; Kilibarda, N.; Cobanovic, N. Safety Aspects of Nanotechnology Applications in Food Packaging. *Procedia Food Sci.* 2015, *5*, 57–60.
- [13] Ibrahim, R. K.; Hayyah, M.; Alsaadi, M. A.; Hayyan, A.; Ibrahim, S. Environmental Application of Nanotechnology: Air, Soil, and Water. Sci. Pollut. Res. Int. 2016, 14, 13754–13788.
- [14] Adam, M. A.; El-Shafey, S. E.; Mohamed, S. R. Enhancing the Performance of SILRES® BS OH 100 as a Consolidant of Archaeological Limestone Using Nano-Hydroxyapatite. *Egyptian J. Chem.* 2023, 66 (10). DOI:10.21608/EJCHEM.2023.179271.7276
- [15] Mohamed, E. H. Effectiveness Assessment of Paraloid B72 Enhanced with Nanomaterials to Improve Mortars Properties for Conservation of Seti I Temple in Al-Qurna, Thebes West Bank, Egypt; South Valley University: 2023. DOI:10.21203/rs-2409498/v2
- [16] Vaz, M. F.; Pires, J.; Carvalho, A. P. Effect of the Impregnation Treatment with Paraloid B-72 on the Properties of Old Portuguese Ceramic Tiles. *J. Cult. Herit.* 2008, *9*, 269–276.
- [17] Mostafa, H. Y.; Hussain, A. I.; El-Mas, A. M. Effect of Monomer Concentration on the Properties of Poly (Methyl Methacrylate/Butyl Acrylate/Vinyl Silica) Emulsion Nanocomposite. *J. Faculty of Science, Zagazig Univ.* 2016. Retrieved from https://journals.ekb.eg/article-31067632ed03
- [18] La Russa, M.; Ruffolo, S. A. F.; Malagodi, M.; Coliviero Rossi, C.; Palermo, A. M. G.; ZaTig, H. Antimicrobial Stone Coating with TiO₂ Powders: An Application on Jalaroid 72. *Appl. Phys.*, 2012, *100*, 829–834.
- [19] Al-Dosari, M. A.; Darwish, S. S.; Adam, M. A.; Elmarzugi, N. A.; Al-Mouallimi, N.; Ahmed, S. M.; Mansour, S. Effects of Adding Nanosilica on Performance of Ethyl Silicate (TEOS) as Consolidation and Protection Materials for Highly Porous Artistic Stone. *J. Mater. Sci. Eng. A* 2016, 6 (7–8).
- [20] Al-Dosari, M. A.; Darwish, S. S.; Adam, M. A.; Elmarzugi, N. A.; Ahmed, S. M.; Mansour, S. Evaluation of Preventive Performance of Kaolin and Calcium Hydroxide Nanocomposites in Strengthening Outdoor Carved Limestone. *Archaeol. Anthropol. Sci.* 2019, *11*, 3389–3405.

476 M. Adam et.al.

- [21] Bakr, A. M. Evaluation of the Reliability and Durability of Some Chemical Treatments Proposed for Consolidation of So-Called Marble Decoration Used in 19th Century Cemetery (Hosh Al Basha), Cairo, Egypt. J. Arab Archaeol. Union 2011, 12, 75–90.
- [22] Helmi, F. M.; Hefni, Y. K. Using Nanocomposites in the Consolidation and Protection of Saudi Stone. Int. J. Conserv. Sci. 2016, 7, 29–40.
- [23] Mahmoud Abd El Hafez. Characterization and Restoration Recommendations of Some Adobe Shrines at El Bagawat Cemetery, Kharga Oasis, Western Desert—Egypt. Egyptian J. Archaeol. Restor. Stud. (EJARS) 2018, 8 (1).
- [24] Seedstudio. USB Digital Microscope. 2017. http://www.seedstudio.com/usbdigitl-microscopep1406.html
- [25] Binici, H.; Binici, F.; Akcan, M.; Yardim, Y.; Mustafaraj, E.; Corradi, M. Physical–Mechanical and Mineralogical Properties of Fired Bricks of the Archaeological Site of Harran, Turkey. *Heritage* 2020, *3* (3), 1018–1034. DOI:10.3390/heritage3030055
- [26] Mahmoud Abd El Hafez. A Diagnostic Study of the Construction Techniques and Materials of the Fatimid Adobe Wall of Cairo, and the Proposed Restoration and Rehabilitation Methodology. J. Faculty Archaeol. Cairo Univ. 2024, 27. (Arabic)
- [27] Pedreschi, R. A Feasibility Study of Post-Tensioned Stone for Cladding. *Constr. Build. Mater.* 2013, *43*, 225–232. DOI: 10.1016/j.conbuildmat.2013.01.030
- [28] ISO. Colorimetry: Part 4: CIE, 1976 Lab Colour Space*; ISO 14-41E, Geneva, 2007.
- [29] Helmi, F. M. Hesniy. A Simple Method for Measuring the Static Water Contact Angle for Evaluation of the Hydrophobicity of the Consolidating and Protective Materials. In *Proceedings of the 1st International Conference of Egypt and Mediterranean Countries Through Ages*, Cairo, Egypt, October 15–18, 2014; Vol 3, pp 327–341.
- [30] Mahmoud Abd El Hafez M. Adam. Archaeometric Study and Restoration Implementation of Archaeological Roman Adobe Bath at Karanis–Fayoum. *Adv. Res. Conserv. Sci.* 2023, 4(1). DOI:10.21608/arcs.2023.186506.1034
- [31] Normal, R. MisureColorimetricheStrumentali di SuperficiOpache; Self-published: Roma, 2017.
- [32] UNI 11207. Cultural Heritage—Natural and Artificial Stones—Determination of Static Contact Angle on Laboratory Specimens, 2007.
- [33] Cappelletti, G.; Fermo, P. Hydrophobic and Superhydrophobic Coating for Limestone and Marble Conservation. In *Smart Composite Coating and Membranes*, El Sevier: Amsterdam, Netherlands, 2016; pp 421–442.